Neuroscience 160 (2009) 784–795

EphB2 AND EphA4 RECEPTORS REGULATE FORMATION OF THE PRINCIPAL INTER-HEMISPHERIC TRACTS OF THE MAMMALIAN FOREBRAIN

S. K. Y. HO,[a] N. KOVAČEVIĆ,[b] R. M. HENKELMAN,[c] A. BOYD,[d] T. PAWSON[e] AND J. T. HENDERSON[a]*

[a]*Department of Pharmaceutical Sciences, Leslie Dan Faculty of Pharmacy, University of Toronto, 144 College Street, Room 903, Toronto, ON, Canada M5S 3M2*

[b]*Rotman Research Institute, Baycrest, 3560 Bathurst Street, Toronto, ON, Canada M6A 2E1*

[c]*Mouse Imaging Centre, Hospital for Sick Children, Toronto Centre for Phenogenomics, 25 Orde Street, Toronto, ON, Canada M5T 3H7*

[d]*Leukemia Foundation Research Laboratory, the Queensland Institute of Medical Research, 300 Herston Road, Brisbane, Queensland 4029, Australia*

[e]*Samuel Lunenfeld Research Institute, Mount Sinai Hospital, 600 University Avenue, Toronto, ON, Canada M5G 1X5*

Abstract—Previously, we have demonstrated that EphB2 activity is required for proper development of the posterior branch of the anterior commissure (ACpp) within the mammalian forebrain. In the present study, using magnetic resonance imaging (MRI), immunohistochemistry, and *in vivo* stereotactic fluorescence tracing of *EphB2, B3, A4* and combinatorial Eph receptor mutants, we have developed a detailed three-dimensional model of how EphB-class receptors interact to regulate commissural formation within the forebrain. The results demonstrate that EphB2 and EphA4 each regulate distinct aspects of axon guidance within the ACpp. Specifically, while EphB2 is required to retard ACpp axons from projecting aberrantly into the ventral forebrain, EphA4 is required to restrict axons from entering the anterior branch of the anterior commissure (ACpa). Together, EphB2 and EphA4 act synergistically to prevent a subpopulation of axons within the anterior branch of the AC from mis-projecting caudally. Analysis of *EphA4* null mice using high resolution MRI reveals for the first time that, in addition to errors in midline guidance, loss of EphA4 results in aberrant lateral and ventral displacement of the ACpa tract. In addition, tracing studies in *α-chimerin* null mice reveal that EphA4-mediated effects are not regulated through this pathway. Taken together, the results demonstrate that each of the principal guidance decisions within both anterior and posterior tracts of the anterior commissure can be accounted for by the individual and combinatorial actions of EphB2/A4 receptors.

Key words: anterior commissure, axon guidance, Eph, MRI.

Proper assembly of the mammalian CNS is critically dependent upon the ability of projecting axons to appropriately innervate their targets (Dodd and Jessell, 1988). Over the past decade, several conserved families of molecules have been identified as important regulators of developmental CNS axon guidance, including the Robo/Slits family members (Brose et al., 1999; Dickson and Gilestro, 2006), netrins/semaphorins (Castellani and Rougon, 2002; Negishi et al., 2005) and Eph/ephrins (Wilkinson, 2000). The largest of these are the Eph family of receptor tyrosine kinases, of which 16 members have presently been identified in vertebrates (Pasquale, 2004). The Eph family can be divided into two broad subgroups based upon the nature of their ligands. EphA receptors primarily interact with ligands which are bound to the cell surface via glycosylphosphotidyl inositol linkages (ephrinAs), while EphB receptors typically interact with cell surface ligands containing both transmembrane and cytoplasmic domains (ephrinBs) (Palmer and Klein, 2003; Pasquale, 2004). Several exceptions to these class rules are known, such as the ability of EphA4 to interact with ephrinB2 and B3 (Gale et al., 1996). Similarly, it has also been demonstrated that the EphB2 receptor exhibits affinity toward ephrinA5 (Himanen et al., 2004). This overlap in binding specificity between subclasses suggests shared activities and potential functional redundancy among family members.

The majority of *in vitro* and *in vivo* studies on Eph receptor function point to the induction of repulsive interaction upon the binding of Eph or ephrin ligands (O'Leary and Wilkinson, 1999); although attractive interactions mediated by each group are known to exist (Davy and Robbins, 2000; Gao et al., 2000; Zhou et al., 2001; Hindges et al., 2002; Mann et al., 2002; Palmer et al., 2002; Davy and Soriano, 2005). Eph receptors are unique among receptor tyrosine kinases in that, in addition to interacting with a cell-bound ligand, significant activation of the receptor does not occur in the dimeric state; but instead requires higher order association (Day et al., 2005; Pabbisetty et al., 2007). Binding of ephrin ligands to the Eph receptor ectodomain, results in the induction of conformational changes which induce receptor activation. Upon activation, Eph receptors autophosphorylate key tyrosine residues within both kinase and juxtamembrane domains (Wybenga-Groot et al., 2001). Receptor phosphorylation induces a transient reduction in RasGAP activity, ultimately triggering local destabilization of the actin cytoskeleton resulting in neuritic retraction (Elowe et al., 2001). In addition to classical forward signaling through the Eph-expressing cell, Eph/ephrin binding can induce signal transduction via ephrin-expressing cell, known as the reverse

*Corresponding author. Tel: +1-416-946-3090; fax: +1-416-978-8511.
E-mail address: jeff.henderson@utoronto.ca (J. T. Henderson).

Abbreviations: AC, anterior commissure; ACpa, anterior commissure pars anterior; ACpp, anterior commissure pars posterior; DKO, double knockout; DM, deformation magnitude; E, embryonic day; MRI, magnetic resonance imaging; PBS, phosphate-buffered saline.

0306-4522/09 $ - see front matter © 2009 IBRO. Published by Elsevier Ltd. All rights reserved.
doi:10.1016/j.neuroscience.2009.03.013

signaling (Henkemeyer et al., 1996; Cowan and Henkemeyer, 2002).

Eph receptors have previously been shown to regulate several developmental processes which include cell migration (Wang and Anderson, 1997; Batlle et al., 2002), tissue patterning (Knoll et al., 2001; Davy and Soriano, 2007), angiogenesis (Gale et al., 2001) and axon guidance (Henkemeyer et al., 1996; Wilkinson, 2001; Palmer and Klein, 2003). Within the mammalian CNS, Eph receptors have been shown to play a role in the guidance of axons within the retinotectal (Frisen et al., 1998), corticospinal (Dottori et al., 1998), thalamocortical (Dufour et al., 2003), vomeronasal (Knoll et al., 2001), vestibular (Cowan et al., 2000), entorhino-hippocampal tracts (Stein et al., 1999; Yue et al., 2002; Chen et al., 2004; Otal et al., 2006) and the anterior commissure (AC) (Henkemeyer et al., 1996). The AC represents a primary inter-hemispheric tract for neurons within the rodent forebrain, and is required for bidirectional communication between components of the anterior aspects of the cerebral hemispheres. The AC is composed of two principal tracts: the anterior commissure pars anterior (ACpa), which communicates between the olfactory lobes, and the anterior commissure pars posterior (ACpp) which principally connects aspects of the temporal lobe. Previously, we have shown that loss of EphB2 results in a significant reduction of the pars posterior axons and that axon guidance was mediated by ephrinB-induced reverse signaling. EphA4 has also been shown to be expressed adjacent to the AC tract, and it has been suggested that mice lacking EphA4 exhibit reductions in AC axons (Dottori et al., 1998; Greferath et al., 2002); however the precise nature of these defects is unknown.

In the present study, we examined the nature of axon decision making in both single and combinatorial *EphB2*, *B3* and *A4* null mice and controls in several different genetic backgrounds. For the first time, we have analyzed and quantified axonal guidance defects within the forebrain of these Eph mutants in an interactive, non-destructive and three-dimensional manner. To determine the detailed three-dimensional structure of all axon tracts within the forebrain with respect to surrounding structures, we have performed high resolution magnetic resonance imaging (MRI) on whole brains. To identify the anatomic origin leading to aberrant AC projections, we have stereotactically labeled the relevant neural fields *in vivo*, via microinjection of fluorescent neural tracers. Using these methods, in combination with immunohistochemistry, a systematic morphologic analysis of the inter-hemispheric connections of the forebrain of each single and combinatorial mutant set was performed. The results obtained reveal the central role of EphB2 and A4 in regulating each of the axon guidance decisions required for neurons innervating both the anterior and posterior tracts of the AC.

EXPERIMENTAL PROCEDURES

Animals

Animals lacking *EphB2*, *EphB3* and *EphA4* genes were generated from the appropriate intercrosses and identified as previously described (Henkemeyer et al., 1996; Dottori et al., 1998). Mice homozygous for the null allele of *EphB2* gene are designated $EphB2^{-/-}$, whereas mice homozygous for a targeted mutation of *EphB2* lacking the kinase, SAM and PDZ-binding motif are designated $EphB2^{N2/N2}$, as previously described (Henkemeyer et al., 1996). Adult *EphB2*, *EphB3*, *EphA4* and combinatorial lines were housed in our conventional animal colony at Mount Sinai Hospital in a controlled environment with a 12-h light/dark cycle. All procedures performed conformed to University of Toronto and the Canadian and Ontario Animal Care Guidelines and were conducted with the aim of minimizing the number of animals used and any acute discomfort.

Stereotactic labeling

Adult animals were anesthetized with 2.5% Avertin (180 μL/10 g body weight) via i.p. injection. Once anesthetized, the scalp was shaved and an incision was made along the dorsal midline. Murine heads were secured for stereotactic procedures using a standard Cunningham mouse stereotactic unit (Cunningham and McKay, 1993). Following proper alignment of the head, placements were made according to the coordinate system we have previously described, obtained from a three-dimensional stereotactic atlases we have developed (Chan et al., 2007) appropriated for the genetic background under study. At the appropriate location, a 500 μm diameter hole was made using a carbide-tipped dental drill. Based upon our cranial alignment scheme (Chan et al., 2007), the following coordinates were employed: (temporal cortex) X: 0.40 mm rostral from bregma, Y: +3.75 mm lateral from midline, Z: 3.77 mm ventral from the dura; (olfactory bulb) X: 4.15 mm rostral from bregma, Y: +0.84 mm lateral from midline, Z: 1.25 mm ventral from dura. Following interruption of the underlying dura, 100–150 nl of fluorescent tracers (DiI or Emerald Green—Molecular Probes) was injected into the target site (temporal cortex or olfactory bulb). To examine interaction of anterior and posterior axons of the AC, both single and dual (cortical/olfactory bulb) stereotactic placements were performed on the same side of the head. Dyes were delivered using a sealed oil microinjection system connected through a microelectrode housing to a borosilicate glass microcapillary with an outer diameter of 50 μm. Following delivery of the neural tracers, the capillary was held in place for 3 min, and then slowly retracted to avoid dye displacement. The incision was sutured closed, and the animals were allowed to recover for 72 h, at which time they were sacrificed and the brains were removed for analysis.

Specimen and image preparation

Animals were euthanized by an overdose of 2.5% Avertin (Miao et al., 2005). Upon the loss of deep tendon responses, mice were transcardially perfused with 0.1 M phosphate-buffered saline (pH 7.4; 0.9% NaCl) (PBS) to flush out vascular fluids, followed immediately by 4% paraformaldehyde in PBS at room temperature (25 °C). Following perfusion, brains were excised and post-fixed in 4% paraformaldehyde in 0.1 M PBS overnight at 4 °C. Specimens for MR imaging were removed from fixative, flushed, and placed into borosilicate tubes filled with a proton-free susceptibility-matching fluid (fluorinert FC-77, 3 M Corp, St. Paul, MN, USA) and imaged as indicated below. Specimens for histologic analyses were equilibrated in 30% sucrose and embedded in Tissue-Tek OCT (Somagen, Torrance, CA, USA). Thirty micrometer frozen sections were obtained on a Leica, CM3050S cryostat and analyzed using a Nikon Eclipse E1000 motorized microscope equipped with a 270° rotating stage, a Hamamatsu C4742-95 camera, Nomarski contrast optics, and fluorescent excitation and emission filters appropriate for the detection of chromophores in the ranges of: DAPI, EGFP, FITC/Cy2, TRITC/Cy3, and Cy5 (excitation/emission filters used for data shown were EGFP: EX-470, EM-525 and TRITC/Cy3: EX-528, EM-600). Dual color fluo-

rescent images shown represent direct composites from the single channel images using Adobe Photoshop 7.0 software.

MR imaging

Specimens were imaged at the Mouse Imaging Centre (MICe), Hospital for Sick Children in a 7.0 T, 30 cm bore magnet (Magnex Scientific, Oxford, UK) with a 27 cm inner bore diameter gradient set (Tesla Engineering, Ltd., Storrington, Sussex, UK) and connected to a Unity^{INOVA} console (Varian Instruments, Palo Alto, CA, USA). Two custom-built, 12 mm, non-uniform solenoid coils were used to image two brains in parallel. The parameters used in the brain scans were optimized for greatest contrast between grey matter and white matter in the mouse brain at 7.0 T (Guilfoyle et al., 2003): T_2-weighted, three-dimensional spin-echo sequence, with TR/TE=1600/35 ms, single average, field-of-view=12×12×24 mm and matrix size=200×200×400 giving an image with an isotropic resolution of 60 μm^3. The total imaging time was 18.5 h.

Image registration and analysis

Image sets were registered as described previously (Kovacevic et al., 2005). Briefly, individual brain images in a given group were first registered and normalized to the average global size, shape and, MR intensity using a nine-parameter affine registration method (Woods et al., 1998), and the software package AIR5.2.2 (University of California). Subsequently, non-linear alignments were performed using the multi-resolution, multi-scale animal methodology initially developed at the Montreal Neurological Institute (MNI) (Kovacevic et al., 2005). Using this procedure, individual image matrices were compared (deformed into) the appropriate control average. Results of this process were recorded in terms of deformation field values, a vector field which described the magnitude and direction of the transformation required at any one point to match a particular region of the individual image to the averaged image (Kovacevic et al., 2005). Relative magnitudes of the spatial transformation are displayed referenced to a spectral color scale, with cool colors (purple) indicative of low levels of spatial variability, and warm colors (red) indicative of high spatial displacement.

3D image reconstruction of the AC

Following registration of the image sets, MRI-identifiable anatomical structures of the AC were automatically delineated as previously described (Kovacevic et al., 2005). Structures comprising the forebrain were additionally cross-checked through manual delineation in each of the three orthogonal planes; using the software package Display (Montreal Neurological Institute, Montreal, Canada). Nomenclature of the structures herein was based upon the nomenclature of Franklin and Paxinos (1997) (Academic Press, San Diego, CA, USA). Two-dimensional visualizations of the results obtained were made using Display/Register (Montreal Neurological Institute). Three-dimensional surface renderings of the data were constructed using AMIRA (TGS, San Diego, CA, USA).

Immunostaining/histochemistry

Embryonic (E) or postnatal (P) brains of the indicated date were dissected and fixed overnight at 4 °C in 4% paraformaldehyde in PBS (0.1 M phosphate buffer, 0.9% NaCl, pH 7.4); then transferred to 30% sucrose, and embedded in OCT (Tissue-Tek). Thaw mount cryostat sections at 16 μm were then collected and allowed to dry at 4 °C overnight. Sections were washed with PBS and blocked in 5% serum and 0.2% tween-20 for 30 min prior to overnight incubation with the designated primary antisera at 4 °C. Antisera utilized for these studies were as follows: anti-ephrinA1, A2 (1:25; Santa Cruz Biotechnology, Santa Cruz, CA, USA), anti-EphA4 (1:20; R & D Systems, Minneapolis, MN, USA), anti-beta-galactosidase (1:200; Promega, Madison, WI, USA). Following washes, sections were incubated with fluorescent secondary antisera at a dilution of 1:200 for 2 h prior to visualization.

For lacZ staining, tissues were fixed for 20 min in 0.2% glutaraldehyde, 5 mM EGTA, 2 mM $MgCl_2$ in 0.1 M phosphate buffer, rinsed three times in wash buffer (2 mM $MgCl_2$, 0.02% NP-40 in PB) and incubated at 37 °C in lacZ staining buffer (wash buffer containing 1 mg/ml X-Gal (MBI Fermentas), 2.12 mg/ml potassium ferrocyanide, and 1.64 mg/ml potassium ferricyanide) until developed. Tissues were rinsed with 0.1 M $NaCO_3$ to stop lacZ development for 15 min. Tissues were postfixed in 4% paraformaldehyde in PBS.

RESULTS

MRI analysis of the CNS structures in *Eph* mutant mice

As a first step to characterize the nature and position of any anatomic anomalies within the brains of our *Eph* mutants, high resolution MRI was performed on both mutants and control littermates. MRI examines the relative differences in local water and lipid content compared to surrounding cell soma (Neema et al., 2007). It is ideally suited for this study because it allows for non-destructive visualization of axon tracts *in situ* and detection of structural deviations observed within a given sample to be later examined histologically.

This method has been recently utilized to detect and quantify changes in axonal organization within the murine CNS that are due to genetic manipulation in mice (Mori and Zhang, 2006; Nessler et al., 2007; Park and Lee, 2007). For *Eph* mutants and controls, raw MRI data sets were collected at a resolution (voxel size) of 60 μm^3. As an initial check of the fidelity and resolution of the system, we first examined our previously characterized *EphB2*$^{-/-}$ mutant (Henkemeyer et al., 1996), in order to compare the MR results obtained with those determined histologically. Consistent with our previous findings, MR imaging of *EphB2*$^{-/-}$ mutants revealed a substantial reduction in the extent of the ACpp (>85% $P<0.001$) (Fig. 1C, G: 3D representation) compared to *EphB2*$^{+/-}$ mutants (Fig. 1B, D: 3D representation). In conjunction with our previous MR atlases of the natural variation in murine strains (Chen et al., 2006), these results validate the utility of the MR parameters employed to examine axon tracts *in situ*; and provide an internal test of the true dimensional limits to which changes in fine tract structure could be determined.

As described previously (Kovacevic et al., 2005), MR-identifiable structures within the brain were compared between mutants, littermate, and atlas controls (Chen et al., 2006) with respect to two fundamental properties: (1) the total volume of the indicated structure (μm^3), and (2) the position of the given neural structure relative to surrounding structures. Positional changes in CNS loci obtained from MR data are represented as the deformation magnitude (DM). DM captures the magnitude and direction of anatomical differences among individual CNS loci and translates the displacement in micrometers into a relative colorimetric scale (Fig. 1J). Together, these analyses

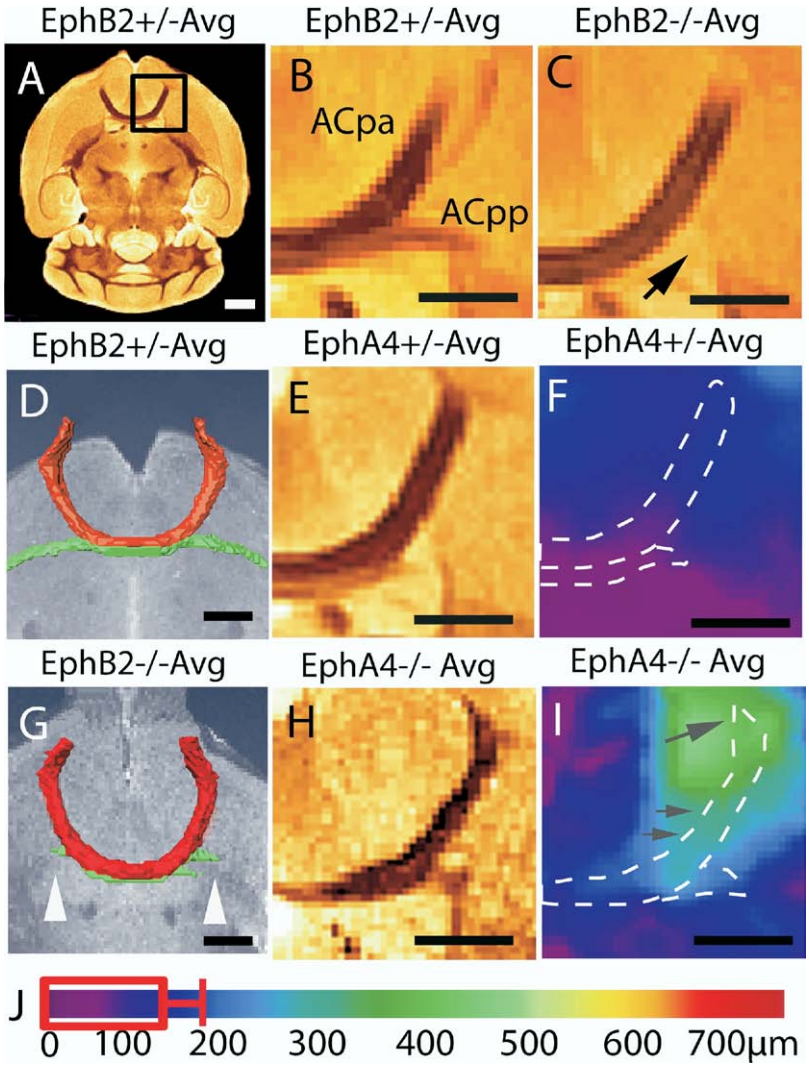

Fig. 1. Analysis of *EphB2* and *EphA4* mutants using high-resolution MRI. Horizontal views of the adult CNS at the level of the AC of $EphB2^{+/-}$ (A, B, D), $EphB2^{-/-}$ (C, G), $EphA4^{+/-}$ (E, F), and $EphA4^{-/-}$ (H, I) mice. An overview of the forebrain is shown in A. Box in A delineates the region of AC represented in the raw MR images and DM maps. The DM is a measure of the magnitude of positional changes within a CNS structure of mutant compared to controls MR images and represents the displacement (in μm) into a colorimetric scale. Areas with warm colors represent regions with large displacements compared to the natural variational average, while cooler colors denote regions with lower relative levels of displacements. (B) Average $EphB2^{+/-}$ image showed normal AC tracts. (C) In contrast, average $EphB2^{-/-}$ image displayed a significant loss of the ACpp, consistent with previous characterization of these mutants using histology (black arrow). 3D reconstruction of the AC for average $EphB2^{+/-}$ (D) and average $EphB2^{-/-}$ (G) MR images demonstrated similar defects in the ACpp as in histologic analyses (white arrowheads), confirming the fidelity and resolution of the MRI system. Raw average $EphA4^{+/-}$ (E) and $EphA4^{-/-}$ (H) MR images showed normal overall AC structure. DM from individual $EphA4^{+/-}$ MR images (n=8) against the control average image (F) and mutant MR images (n=8) against the control average image (I) are illustrated as a color coded map. In these panels, the relative positions of the AC tract from the corresponding MR view are indicated by a dotted line. (I) Displacements of ~200–400 μm are evident in the ACpa $EphA4^{-/-}$ compared to controls (grey arrows representing vectors of deformation). Note the apparent loss of ACpp density in the $EphA4^{-/-}$ mice (arrowhead in H) compared to $EphA4^{+/-}$ (E). (J) Spectral color scale for DM analyses with units in microns (F, I). The boxed region indicates the level of variability seen among $EphA4^{+/-}$ controls ((heterozygotes compared against the heterozygous average) ±SEM at $P<0.05$). Scale bars=1 mm. For interpretation of the references to color in this figure legend, the reader is referred to the Web version of this article.

helped define the nature, extent, and significance of any structural deviations observed within mutant versus control comparisons. With the exception of the reductions seen in the ACpp, no additional structural anomalies were observed by MRI within the forebrain of $EphB2^{-/-}$ mutants (n=7). Analysis of MRI data from $EphA4^{+/-}$ mice also demonstrated no significant differences compared to wild-type littermates or 129S1/SvImj atlas controls ($n \geq 8$ mice per genotype, data not shown). As shown in Fig. 1E, F, $EphA4^{+/-}$ mice exhibit a morphologically normal AC, with little variation (<150 μm) among individuals with respect to either the AC or surrounding structures in comparison to the composite average (Fig. 1F) (n=8). By contrast, all $EphA4^{-/-}$ mice (n=8) exhibited substantial variation in several regions of the AC (Fig. 1I) with respect to the relative position of the AC (indicated by DM up to 400 μm

in Fig. 1I) to the surrounding CNS structures. However, the total volume of the ACpa was not significantly different ($P=0.13$) in *EphA4*$^{-/-}$ mice versus *EphA4*$^{+/-}$ controls (0.42 ± 0.10 versus 0.5 ± 0.05 mm^3 respectively). Within the ACpp, however, *EphA4*$^{-/-}$ mice exhibited a 43% reduction in tract volume compared to heterozygous controls (0.15 ± 0.05 versus 0.27 ± 0.04 mm^3 respectively, $P<0.01$).

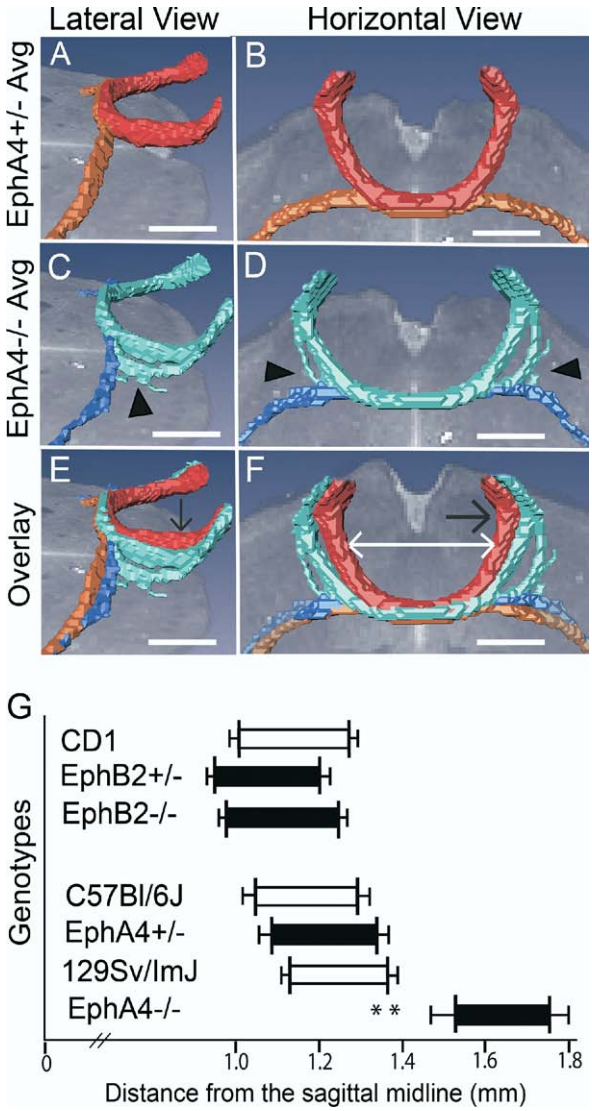

Fig. 2. Three-dimensional representations of the AC in *EphA4* mice. (A–D) Three-dimensional renderings of the AC for *EphA4*$^{+/-}$ (A, B) and *EphA4*$^{-/-}$ (C, D) mice are shown in lateral and horizontal views respectively. (E, F) Heterozygotes average/homozygote average overlays in the lateral and horizontal views respectively. Note *EphA4*$^{-/-}$ mice exhibit tract deviations within the ACpa (arrowheads in C, D), a ventral shift in ACpa (black arrow in E), and enhanced lateral displacement in ACpa (black arrow in F) compared to *EphA4*$^{+/-}$ littermate controls. Scale bars=1 mm (A–F). (G) Analysis of ACpa tract width at midway between its caudal limit and the cortical boundary (white arrow in F). Each bar corresponds to the averaged width of the ACpa tract for each genotype. The bar on the left end represents the mean (±SEM) distance to the inside boundary of the ACpa, while the bar on the right end is the mean (±SEM) distance to the outside boundary of the ACpa (** $P<0.01$; *t*-test).

To better understand the nature of the morphologic defects induced by EphA4 deficiency, three-dimensional representations of the entire AC were generated for all *EphA4*$^{-/-}$ mutants and controls. In contrast to wild-type and *EphA4*$^{+/-}$ littermates (Fig. 2A, B), EphA4$^{-/-}$ mice (Fig. 2C, D) showed perturbations in both the distribution and axonal organization of the ACpa tract (Fig. 2C, D arrowheads). Tract perturbations reminiscent of de-fasciculation are a common feature in EphA4$^{-/-}$ mice along the caudal aspect of the ACpa tract (arrowhead). The full magnitude of these perturbations of the ACpa tract can be seen in the *EphA4*$^{-/-}$/*EphA4*$^{+/-}$ overlays (Fig. 2E, F). To determine the relative morphologic significance of the increase in ACpa tract displacement from the midline seen in *EphA4*$^{-/-}$ mice, this distance was determined for *EphB2* and *A4* mutants and controls, together with CD1 ($n=10$), C57BL/6J ($n=10$) and 129 S1/SvImj ($n=10$) wild-type (WT) mice. The ACpa in *EphA4*$^{-/-}$ mice exhibited a lateral displacement of greater than 400 μm from the midline compared to *EphA4*$^{+/-}$ mice (Fig. 2G). This lateral displacement of the ACpa from the CNS midline is fairly consistent across a number of genetically different comparator groups (Fig. 2G). This displacement is significantly increased in *EphA4*$^{-/-}$ mice compared to each of the comparison groups, consistent with the DM results for these mutants (Fig. 1I).

Disruption of axon path finding in EphB-family mutants

As indicated above, the MRI parameters used provided a means to quantitatively analyze global positional and/or structural changes in MR-definable objects of sufficient magnitude. However, to understand the mechanisms by which these deviations arise, it was necessary to clearly determine the path of axons innervating each AC tract. We therefore performed simultaneous stereotactic microinjections of different fluorescent neural tracers into anesthetized wild-type and *EphB* family mutants into sites within the temporal cortex and olfactory bulb. Tracing was performed for a period of 4 days, at which time animals were sacrificed and serially sectioned in the horizontal (transverse) plane. Temporal and olfactory microinjections of *EphA4*$^{+/-}$ (Fig. 3A) and wild-type (data not shown) mice showed robust labeling and distinct axonal pathways by the ACpp and ACpa tracts, respectively. Tracing studies performed in *EphB2*$^{-/-}$ mice revealed a substantial reduction in ACpp axons (Fig. 3B), consistent with previous observations (Henkemeyer et al., 1996). Those axons which do arrive at the midline in *EphB2*$^{-/-}$ mice, however, persist in forming a discreet ACpp tract which crosses the midline properly (Fig. 3B). In contrast, ACpp axons in *EphA4*$^{-/-}$ mice exhibit aberrant axon guidance upon contact with ACpa axons (Fig. 3C–E) where the ACpp axons in these mice now freely intermingle with those of the ACpa tract. As a result, in *EphA4*$^{-/-}$ mice, approximately one-half of all ACpp axons become misdirected along the ACpa tract (Fig. 3D); while the remainder exit the midline and resume projection to the contralateral hemisphere. Interestingly, as shown in the progressively more ventral levels

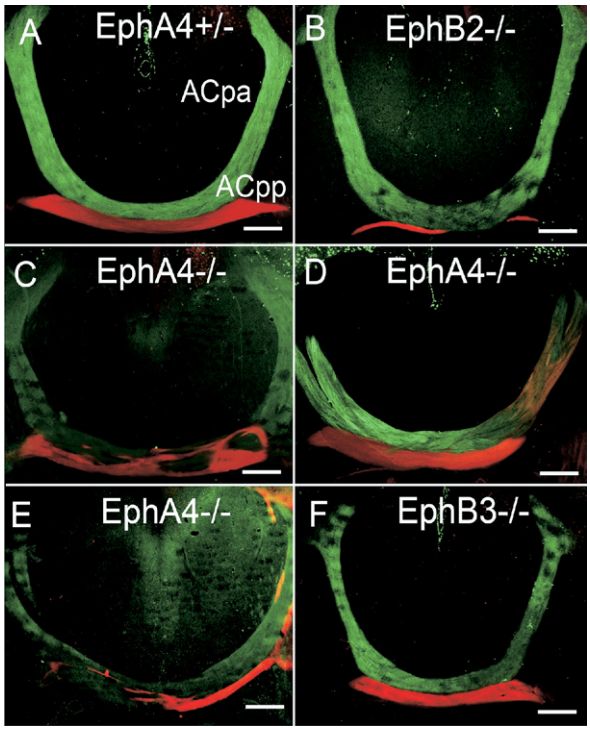

Fig. 3. Axonal path-finding defects in *Eph* family mutants. (A–F) Fluorescent tracers were employed to map the *in vivo* axonal distribution within the component tracts of the AC, following stereotactic injection in the olfactory (green) or temporal (red) compartments. (A) Fluorescent labeling of the AC in *EphA4*$^{+/-}$ mice shown in the horizontal plane. (B) Labeling in *EphB2*$^{-/-}$ mice, demonstrating the reduction in ACpp labeling. (C–E) Labeling pattern seen in three independent *EphA4*$^{-/-}$ mice, showing progressively more ventral planes within the AC to demonstrate intermingling of ACpp axons with those of the ACpa tract. (F) Tract labeling observed in *EphB3*$^{-/-}$ mice. Scale bar=400 μm (A–F). For interpretation of the references to color in this figure legend, the reader is referred to the Web version of this article.

of the AC among different *EphA4*$^{-/-}$ mice (Fig. 3C–E), the character of ACpp and ACpa intermingling changes and becomes more stratified within the ventral AC. The aberrant behavior of ACpp axons in *EphA4*$^{-/-}$ mice as seen by *in vivo* neural tracing is consistent with both the MRI-based volumetric reduction of the ACpp tract, and the disappearance of MR contrast intensity along the AC midline seen in *EphA4*$^{-/-}$ mice (Fig. 1H). Despite this deviation, ACpp axons of *EphA4*$^{-/-}$ mice are still observed to project only along the well-defined tracts of the AC (ACpp, ACpa) rather than projecting randomly within a given zone, as observed for ACpp axons of *EphB2*$^{-/-}$ mice (Henkemeyer et al., 1996). *In vivo* tracing of axons also demonstrates that the apparent tract fasciculation events seen along the caudal aspect of the ACpa tract in *EphA4*$^{-/-}$ mice using MRI, actually represent bundles of mis-projecting ACpp axons which project through the ACpa tract (Fig. 3E). As shown in Fig. 3, aberrant axonal projection is not observed for ACpa axons in *EphA4*$^{-/-}$ mice, similar to *EphB2*$^{-/-}$ mice. With respect to other EphB family members known to be expressed within the forebrain, neural tracing experiments performed using *EphB3*$^{-/-}$ mice (Fig. 3F), and mice homozygous for a targeted deletion of the EphB2 intracellular domain (*EphB2*$^{N2/N2}$; Henkemeyer et al., 1996) (data not shown), show axonal tracing patterns identical to that seen in wild-type and heterozygous controls (Fig. 4A).

Recently, several groups have demonstrated that α-2 chimerin is a downstream target of EphA4, raising the possibility that α-chimerin-mediated signaling may also act to regulate AC formation (Beg et al., 2007). Histologic observation by the authors indicated no gross morphologic perturbations of the AC of *α-2 chimerin* null mutants. However, due to the nature of the targeting defects we ob-

A

Eph	B2	B3	A4	ACpa	ACpp
WT	+/+	+/+	+/+	W	W
Single	-/-	+/+	+/+	W	A1
	+/+	-/-	+/+	W	W
	+/+	+/+	+/-	W	W
	+/+	+/+	-/-	W	A2
B2/B3	+/-	+/-	+/+	W	W
	-/-	-/-	+/+	W	A1
B2/A4	+/-	+/+	+/-	W	W
	-/-	+/+	-/-	A3	A1, 2
N2/A4	N2/N2	+/+	+/+	W	W
	N2/N2	+/+	-/-	W	A2

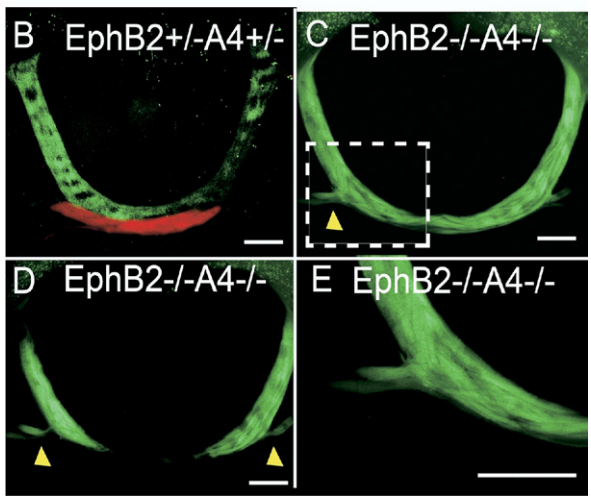

Fig. 4. Synergistic effects of EphB-family receptors. (A) List of combinatorial *EphB*-family mutants and controls examined by *in vivo* stereotactic neural tracing (column headings), together with the ACpp and ACpa phenotypes observed (W, wild type/control pattern; A1, axon path-finding defect typified by *EphB2*$^{-/-}$ mutants; A2, axon guidance defect typified by *EphA4*$^{-/-}$ mutants; A3, synergistic/non-additive axon guidance defect). (B–E) Fluorescent photomicrographs of the AC in the horizontal plane, demonstrating the pattern of labeling observed for EphB2$^{+/-}$A4$^{+/-}$ (B), and *EphB2*$^{-/-}$*A4*$^{-/-}$ mice (C–E). ACpp axon labeling has been removed for clarity. Note that ACpa axons in EphB2$^{-/-}$A4$^{-/-}$ mice become redirected along the intertwined ACpp pathway (arrowheads C and D). (E) Higher magnification example of the ACpa misdirected axons shown in (C). Scale bar=400 μm (B–E).

served in the *EphA4* null mice (which would not be observed histologically), we performed *in vivo* neuro-anatomic tracing in mice homozygous for an inactivating point mutation in the GAP domain of the α-*chimerin* gene (α-*1* and -*2 chimerin* null mutant), to determine whether α-chimerin deletion results in similar axon guidance defects observed for *EphA4* null mice (Iwasato et al., 2007). Analysis of serial sections from the AC from these animals demonstrated that both the anterior and posterior tracts of the AC were normal in α-*1* and -*2 chimerin* null mice (data not shown).

Synergistic regulation of axon guidance by *Eph* family members

As indicated above, genetic deletion of EphB2 and A4 (but not B3), exhibits unique effects on axon guidance within the AC. To examine potential interactions between Eph family members in this system, a series of combinatorial *Eph* mutants was generated (Fig. 4A). As indicated in the figure, with the exception of *EphB2*/*A4* double knockouts (DKO), each of the combinatorial lines examined exhibited either a wild-type pattern of innervation, or recapitulated the phenotype of one of the single knockouts. *EphB2*/*A4* double heterozygotes exhibited wild type patterns of axon guidance in both the ACpa and ACpp (Fig. 4B). While the ACpp axons in *EphB2*/*A4* DKO exhibited an additive pattern of the axon guidance defects seen in *EphB2*$^{-/-}$ and *EphA4*$^{-/-}$ mice, the ACpa axons in DKO animals exhibited a unique pattern of aberrant axon guidance not seen in either of the single null mutants; as shown by axonal tracing. A subgroup of ACpa axons in *EphB2*/*A4* DKO was redirected into the ACpp pathway (Fig. 4C–E). Similar to the behavior seen in *EphA4*$^{-/-}$ mice, misdirected ACpa axons in *EphB2*/*A4* DKO only project along the pathway defined by the ACpp. Thus, while EphB2 and EphA4 regulate distinct aspects of axon path finding in ACpp axons, both receptors participate in regulating the guidance of ACpa axons.

Expression of *Eph* receptors and ephrin ligands in the developing forebrain

Results obtained from MRI and stereotactic tracing analyses of Eph family mutants suggested a mechanism by which these Eph receptors interact to control axon guidance. To further define the nature of these interactions, we examined in three dimensions, the pattern of EphB2 and EphA4 and ephrin ligands expression within the developing forebrain at embryonic day (E) 15, a time at which ACpa and ACpp tracts are still forming. The pattern of EphB2 expression was determined using lacZ histochemistry in *EphB2*$^{N2/+}$ knock-in mice, as previously described (Henkemeyer et al., 1996). In these animals, the β-galactosidase gene is fused with the *EphB2* coding sequence downstream of the juxtamembrane tyrosine residues. The results show that while low levels of EphB2 expression persist dorsal to the principal region of the AC, the domain of highest local EphB2 expression exists just ventral and lateral to the commissural midline under the primary projection path of the AC (Fig. 5A). Within the forebrain, the region of high EphB2 expression extends caudal to the AC, but tapers rostrally beyond the immediate vicinity of ACpp axons (Fig. 5B, 5C). With respect to EphA4, immediately surrounding the midline, high EphA4 expression is observed adjacent to the AC tract consistent with previous reports (Kullander et al., 2001); while more laterally (Fig. 5E, arrow), a roughly triangular domain of elevated EphA4 expression was observed in the region ventrolateral to the AC tract. Together, EphA4 and EphB2 form a pattern of adjacent domains within the mammalian forebrain (summarized in Fig. 5H). Analysis of ephrinB expression using antisera which recognizes ephrinB1/B2, demonstrates that axons within both the pars anterior and pars posterior express ephrinBs (Fig. 5D). Thus, both ACpp and ACpa axons possess (at a minimum) the ability to respond to the effects of EphB2. Within the components of the temporal lobe which gives rise to axons of the ACpp tract, we also observed ephrinB expression (Fig. 5D, arrowhead). Despite previous suggestions that EphB/ephrin signaling may assist in the guidance of cortical axons, none of the single or double mutant combinations examined (Fig. 4A), exhibited significant perturbations in the initial coalescence of the ACpp (or ACpa) tract.

The free intermingling between ACpp and ACpa axons in the absence of EphA4, prompted us to examine the pattern of EphA4 in ACpp and ACpa axons. In wild-type mice, ACpp axons (but not ACpa) expressed EphA4 (Fig. 5E), suggesting a possible mechanism for EphA4-mediated axon sorting between ACpp and ACpa axons during development. The stringent segregation between ACpp and ACpa axons could reflect response to either the coincident contact of growing ACpp/ACpa axons along the CNS midline, or represent a subsequent segregation for late arriving axons. The intermingling of ACpp and ACpa axons seen in *EphA4*$^{-/-}$ mice suggested to us that this deviation might arise as a result of the coincident arrival of ACpp and ACpa axons at the AC junction. We therefore examined the pattern of ACpp and ACpa axon innervation toward the AC junction using lipophilic neural tracers in fixed whole brains from E13.5–E16.5 embryos. For the genetic backgrounds examined, no significant innervation at the AC junction was observed prior to E13.5–13.75. Neural tracings performed at E13–E14.5 suggested coincident or near coincident arrival of ACpp and ACpa projections (Fig. 5G). The data obtained suggest the pattern of Eph/ephrin expression (Fig. 5H), in which a domain of high EphA4 expression lies immediately rostral to that of EphB2. Both axons of the ACpa and ACpp express ephrinB ligands, with axons of the ACpp expressing low levels of EphA4.

DISCUSSION

Previous *in vivo* analyses of Eph/ephrin-mediated axon guidance within the AC by laboratories including our own have largely been confined to gross histologic examination. While such analyses provide a valuable overview of the structural morphology of the AC in genetic mutants, they do not allow the specific origin, innervation or path

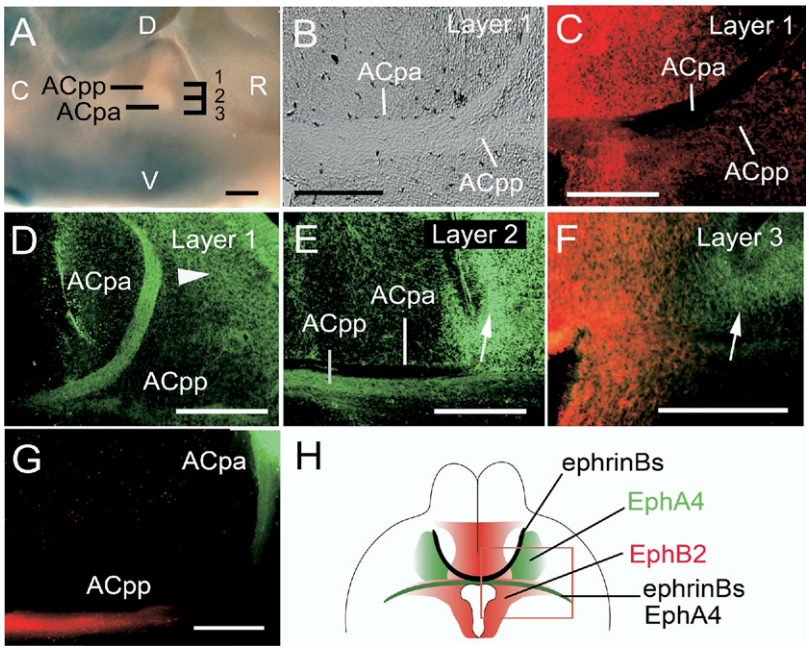

Fig. 5. Eph and ephrin ligands expression in developing forebrain from E13–E16. (A) Pattern of EphB2 expression in *EphB2*$^{N2/N2}$ embryos at E15 shown in the sagittal plane at the level of the midline at the AC in whole mount specimen (N2 designates the allele for *EphB2* gene encoding the fusion of the extracellular and juxtamembrane domains of EphB2 linked to β-galactosidase in place of the EphB2 c-terminus). High level of EphB2 expression was seen lateral and immediately ventral to the AC tract, as shown by β-galactosidase histochemistry. D: dorsal, V: ventral R: rostral, C: caudal. Layers 1–3 represent the approximate level at which the horizontal sections were obtained. (B) Brightfield photomicrograph in the horizontal plane showing the normal projection of the ACpa tract in control forebrain at E15. At this stage of development, the ACpa tract lies just ventral to base of the lateral ventricles. (C) Pattern of anti-beta galactosidase staining in *EphB2*$^{N2/N2}$ embryos at E15 shown in the horizontal plane, illustrating EphB2 expression in the midline and lateral regions below the AC tract. This pattern is consistent with pattern seen in whole mount lacZ staining (A). (D) Pattern of ephrinB1/B2 staining at E15 shown in the horizontal plane. Note that ephrinB expression is observed in both ACpa and ACpp tracts consistent with previous reports (Kullander et al., 2001). (E) Low levels of EphA4 expression in ACpp but not ACpa axons at E15; as shown in the horizontal plane. (F) Pattern of EphA4 (green) and EphB2 (red) expression at E15 shown in the horizontal plane ventral to the AC. High level of EphB2 is observed at midline and ventral caudal to where normally the ACpp passes. (G) Development of ACpa and ACpp axon tracts within the forebrain. Injection of lipophilic tracers into fixed tissues from E13.5–E16.5, demonstrates that axons of the ACpp and ACpa tracts project toward and reach the sagittal midline in a synchronous manner. Section is shown in the horizontal plane at E14.5. (H) Schematic model of the pattern of EphB2 and EphA4 expression observed within the developing forebrain, together with ephrin ligands. With respect to the ACpa tract, the domain of EphA4 expression lies just rostral to the domain of elevated EphB2 expression. Scale bar=200 μm (A–G). For interpretation of the references to color in this figure legend, the reader is referred to the Web version of this article.

taken by individual axons to be determined. To more clearly determine the mechanism by which EphB-type receptors act to control AC axon guidance, we have for the first time performed quantitative 3D MRI of *EphB2*, *B3*, *A4* and combinatorial null mutants in concert with *in vivo* stereotactic tracing.

These results demonstrate that the loss of EphA4 activity results in the development of several previously unrecognized axon guidance defects within the AC; including ACpa, ACpp axon segregation. Specifically, high-resolution MR imaging demonstrates for the first time that loss of EphA4 results in a significant ventral and lateral displacement of the ACpa tract in relation to surrounding forebrain structures compared to both heterozygous and wild-type controls, demonstrating that EphA4 plays an important role in positioning the ACpa tract within the dorsoventral and mediolateral axes. In the absence of a means to definitively globally position fine structures of the AC with a high degree of confidence within the CNS, and without corresponding measures of natural variability, such determinations are difficult to assess with confidence. High-resolution MRI analyses therefore enable a new level of quantitative structural analyses to be performed in the indicated axon guidance mutants.

With respect to guidance cues regulating the interaction of ACpa and ACpp axons at the sagittal midline, analysis of *EphA4* null mutants demonstrates that loss of EphA4 normally expressed in ACpp axons, results in a stochastic intermingling of ACpp axons with those of the ACpa tract. Thus, EphA4 normally regulates the midline segregation of ACpp from ACpa axons during their coincident developmental arrival through a repulsive mechanism. We observe that this aberrant projection persists, continuing into the adult period. It is interesting to note that the degree of tract intermingling appears higher in the central and the dorsal aspect of the AC midline compared to ventral regions, suggesting the potential involvement of additional axon guidance molecules. Beyond the sagittal midline, in *EphA4* null mice, mis-projecting ACpp axons can continue to project along the ACpa tract. However, the converse projection (ACpa axon projection along the ACpp tract beyond the midline) is prohibited. Our expression studies suggest that this difference in axon guidance may relate to the greater sensitivity of ACpa versus ACpp axons

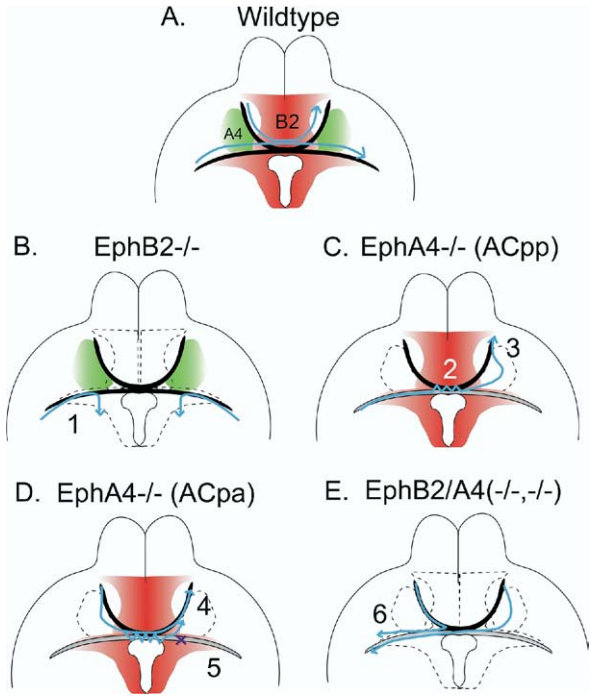

Fig. 6. Eph-mediated interactions within the developing forebrain. Schematic representations of the behavior of axons within the AC based upon the individual and cumulative affects of EphA4 and EphB2 during development. EphA4 (A4) and EphB2 (B2) expression domains and the nature of AC axonal projections within the forebrain of wild type mice are indicated (A). (B) As indicated previously (Henkemeyer et al., 1996), in the absence of EphB2, axons from temporal neurons comprising ACpp tract fail to encounter EphB2-mediated repulsion as they approach the sagittal midline; resulting in aberrant projection to the floor of the forebrain (1). (C) In the absence of EphA4, several axonal deviations occur. Normally, the coincident developmental projection of the ACpp and ACpa tracks results in segregation of ACpp and ACpa axons. In the absence of EphA4, axons of the ACpp exhibit a loss of repulsive contact between ACpa axons, resulting in free intermingling of ACpp and ACpa axons (2). As a result of this intermingling, axons of the ACpp stochastically mix with ACpa axons, ultimately resolving into either continued projections towards the contralateral temporal cortex, or aberrant projection along the ACpa tract (3). Aberrant ACpp axons can either project within the displaced (see below) ACpa toward the rostral forebrain (3), or clusters of ACpp axons can continue along a more lateral course from the midline, due to the absence of EphA4 expression in the region immediately rostral to the EphB2. In such instances, because of the more ventral position of the ACpa tract compared to the ACpp, these axons continue until they encounter the rostral perimeter of the high EphB2 expressing domain. As these axons cannot project caudally due to high levels of EphB2, they turn in an anterior direction, typically rejoining the ACpa tract. (D) With respect to ACpa axons, the absence of EphA4 results in ventrolateral deviation of the ACpa tract (4) due to loss of the forebrain EphA4 domain indicated. In addition, while ACpp and ACpa axons can freely intermingle at the midline, only ACpp axons can project into ACpa territory in the absence of EphA4. ACpa axons are blocked from the converse behavior (ACpp tract entry −5), due to their apparently greater sensitivity to EphB2-mediated repulsion. (E) In the absence of both EphB2 and EphA4, each of the individual guidance errors described above occurs; however in addition, axons of the ACpa can now enter ACpp territory (6) due to removal of the remaining EphB2 barrier. However, in contrast to the stochastic intermingling observed in ACpp axons, only a minority of ACpa axons (~20%) ultimately enter the ACpp tract in the absence of EphB2 and A4.

to EphB2-mediated repulsion. The repulsion of ACpp axons appears to involve the gradient of EphB2 expression seen lateral to the midline within the ACpp tract territory.

In the absence of EphA4 expression beyond the midline segregation point for ACpp and ACpa axons, misprojecting ACpp axons either travel along the main body of the ACpa tract, or continue to proceed laterally until they encounter a region of elevated EphB2 expression (summarized in Fig. 6C). Upon reaching this point, these axons cannot project laterally or caudally due to the high local levels of EphB2. They, therefore, proceed anteriorly, frequently rejoining the ACpa tract at its rostral aspect. As such, the ACpa tract in *EphA4* null mice appears to exhibit de-fasciculated bundles of the ACpa tract. Analysis of stereotactic tracing in such animals demonstrates however that these “de-fasciculated bundles” are in fact composed of mis-projecting ACpp axons. This also explains the true origin of the so-called U-turn projections seen in ACpa axons in *EphA4* null mice, as described previously by Kullander (2001). The present study demonstrates that such projections are not ACpa tract element U-turns, but rather separate ACpp tract elements coalescing just lateral to the sagittal midline.

Taken together, both the genetic ablation and immunohistochemical expression studies support a model where ephrinB expressing ACpa axons are repelled through ventrolateral interaction with EphA4 expressing regions adjacent to ACpa tract (summarized in Fig. 6D). This model suggests that in the absence of rostral EphA4 expression, ACpa axons originate from the piriform cortex of olfactory bulb project ventral and lateral to their normal path, projecting caudally until they reach a zone of high EphB2 expression (Fig. 6D). At this point they are redirected toward the midline (Figs. 6D–4). The loss of this rostral EphA4 domain (Fig. 6C) also allows the ventrolateral deviation of mis-projecting ACpp axons from the midline (see below).

Interestingly, we observed concomitant expression of both EphA4 and ephrinBs expression within axons of the ACpp. Consistent with this, previous reports have demonstrated ephrinB2 expression within the ACpp (Cowan et al., 2004). This poses an intriguing problem with regard to how ACpp axons respond to the dual expression of a given Eph receptors and its ligand within the same tract; as these axons do not appear to exhibit significant self-repulsion. Previous *in vitro* studies have provided evidence of down-regulation of Eph/ephrin signaling *in cis* (Carvalho et al., 2006). Another potential explanation involves mutual exclusivity of EphA4 and ephrinBs. An example of this is seen in the work of Marquardt et al. (2005) who examined EphA and ephrinAs co-expression in motor axons. It was proposed that EphA and ephrinAs were segregated into separate membrane domains and were capable of simultaneously binding their respective partners presented *in trans* (Marquardt et al., 2005). Whether internal repulsion arising from the relatively low levels of EphA4 in ACpp axons (relative to adjacent domains such as the ACpa tract) is overridden by surrounding Eph-ephrin interactions or through the influence of additional signaling molecules remains to be determined. However recently, several laboratories have identified Rac-GTPase α2-chimerin as a key mediator of ephrinB3/EphA4 forward signaling in the

development of motor circuits (Beg et al., 2007; Iwasato et al., 2007; Wegmeyer et al., 2007). Our tracing analysis of these mutants demonstrates that unlike the corticospinal tract, α-1 and -2 chimerin do not mediate the actions of EphA4 with respect to the AC. The fact that our axonal tracings in α-*Chn* null mice did not result in similar phenotype to that seen in *EphA4* knockouts, supports evidence for a reverse signaling mechanism. Consistent with this, reverse signaling through ephrinB2 has previously been shown to mediate the repulsion of ACpp axons from the ventral regions (Cowan et al., 2004).

Analysis of ACpp axons in both *EphB2* and *EphA4* null mice, demonstrates that these similar signaling complexes impart unique guidance activities to this axonal population. From a developmental perspective, it is remarkable that two receptors of such similar structural character with largely overlapping ligand binding and expression profiles should exert such selective control over a given group of axons. Such findings highlight the complex and variegated nature of the Eph/ephrin receptor system. That these signaling interactions are strictly separable with respect to the guidance of ACpp axons is illustrated by the fact that ACpp axons of *EphB2*/*A4* DKO mice exhibit no additional perturbation with respect to axon guidance beyond the addition of each of the single knockout phenotypes.

While we have demonstrated that EphA4 and EphB2 play distinct roles in the guidance of ACpp axons, our analysis of the *EphB2*/*A4* DKO demonstrates for the first time, a synergistic effect for these receptors with respect to the guidance of a subpopulation of ACpa axons. In addition to exhibiting the guidance errors seen in each of the corresponding single knockouts, $\sim$20%$\pm$7% of the ACpa fibers in *EphB2*/*A4* DKO now leave the ACpa tract and enter ACpp territory (Fig. 6D). In contrast to the stochastic behavior (50% of the axons) seen for ACpp axons in *EphA4*$^{-/-}$ mice, the mis-projection seen in the DKO represents approximately half this number, suggesting that functional heterogeneity may exist within the ACpa population. The mis-projection of less than 50% of ACpa axons in *EphB2*/*A4* DKOs suggests that additional guidance molecules may regulate this process. In this respect, it is interesting to note that like the *EphA4* null mutant, mice lacking *Sema3B* also exhibit a ventral and lateral shift in the ACpa tract (Falk et al., 2005). In the absence of a comparable quantitative determination of ACpa tract morphology in *Sema3B* null mutants, it is difficult to determine with certainty whether the extent of these deviations is similar to that seen in *EphA4* null mice. However, the ability of *Sema3B* ablation to phenocopy at least some of the features seen in *EphA4* null mutants suggests that these disparate receptors ultimately act to affect common downstream mechanisms regulating axon guidance. With respect to Eph-mediated axon guidance, the altered projection of ACpa axons seen in the *EphB2*/*A4* DKOs strongly implies that these receptors have compensatory roles in regulating the anterior–posterior guidance for at least some ACpa axons. However, it does not necessarily indicate that they share an identical mode of action, as suggested by their distinct pattern of expression and the differential effects on ACpa tract morphology. As shown in the model, we postulate that in the absence of EphB2, ACpa axons are restricted from entry into the ACpp through interaction with EphA4-expressing ACpp axons at the midline due to their expression of ephrinA3 (Kudo et al., 2005). By contrast, in the absence of EphA4 at the midline, ACpa axons are not formally repelled from entry into the ACpp tract. We demonstrate that at least a subgroup of these axons does not continue along the ACpp tract due to elevated levels of EphB2 expressed lateral and caudal to the midline.

While our analysis of *Eph* mutants identifies their role both alone, or in combination, in regulating the key steps involved in properly guiding forebrain axons to the contralateral hemisphere, these data also highlight the importance of additional regulators in controlling tract formation. In none of the single or combinatorial Eph receptor mutants examined was a complete loss of the ACpa or ACpp tract observed, suggesting the influence of axon guidance molecules in regulating initial projection of AC axons. Consistent with this, mice lacking netrin1 fail to extend axons to either the ACpa or ACpp (Serafini et al., 1996). In addition, the absence of the semaphorin ligand Sema3F (Sahay et al., 2003) or its principal receptor Npn2 (Chen et al., 2000; Giger et al., 2000), results in a substantial reduction in numbers of both ACpa and ACpp axons projecting to the AC. In contrast to the indicated EphB receptors, these additional guidance cues appear to exert a more generalize influence on axonal behavior within the CNS. Thus, while EphB-class receptors regulate discrete aspects of the projection of both ACpa and ACpp axons, as well as tract segregation, the process of commissure formation is influenced particularly with respect to initial projection by an array of additional guidance cues.

In addition to the *Eph* null mutants indicated above, *EphB3* and a series of additional combinatorial null mutants (Fig. 4) were examined with several different murine backgrounds (C57Bl/6J, 129 S1/SvImj, mixed). Within the forebrain *EphB3* null mutants did not exhibit statically significant defects in axon guidance with respect to the analyses performed. Similarly, none of the combinatorial mutants listed demonstrated additional axon guidance defects beyond that which we have described for the indicated single mutants. Taken together, these date provide a basis for understanding the mechanism by which EphB-class receptors regulate not only ACpp axon guidance, but the position and trajectory of the ACpa tract, as well as anterior–posterior tract segregation within the AC. Specifically, EphB2 and A4 exert both unique and synergistic activities with respect to inter-hemispheric connection of the forebrain.

Acknowledgments—We thank Dr. Roder Laboratory for providing us with the α-chimerin transgenic and littermate control mice. This work was supported by funding from the Canadian Institute for Health Research (CIHR), the Amyotrohic Lateral Sclerosis Society of Canada, the Muscular Dystrophy Association of Canada, and the National Alliance for the Research on Schizophrenia and Depression (NARSAD).

REFERENCES

Batlle E, Henderson JT, Beghtel H, van den Born MM, Sancho E, Huls G, Meeldijk J, Robertson J, van de Wetering M, Pawson T, Clevers H (2002) Beta-catenin and TCF mediate cell positioning in the intestinal epithelium by controlling the expression of EphB/ephrinB. Cell 111:251–263.

Beg AA, Sommer JE, Martin JH, Scheiffele P (2007) alpha2-Chimaerin is an essential EphA4 effector in the assembly of neuronal locomotor circuits. Neuron 55:768–778.

Brose K, Bland KS, Wang KH, Arnott D, Henzel W, Goodman CS, Tessier-Lavigne M, Kidd T (1999) Slit proteins bind Robo receptors and have an evolutionarily conserved role in repulsive axon guidance. Cell 96:795–806.

Carvalho RF, Beutler M, Marler KJ, Knoll B, Becker-Barroso E, Heintzmann R, Ng T, Drescher U (2006) Silencing of EphA3 through a cis interaction with ephrinA5. Nat Neurosci 9:322–330.

Castellani V, Rougon G (2002) Control of semaphorin signaling. Curr Opin Neurobiol 12:532–541.

Chan E, Kovacevic N, Ho SK, Henkelman RM, Henderson JT (2007) Development of a high resolution three-dimensional surgical atlas of the murine head for strains 129S1/SvImJ and C57BL/6J using magnetic resonance imaging and micro-computed tomography. Neuroscience 144:604–615.

Chen H, Bagri A, Zupicich JA, Zou Y, Stoeckli E, Pleasure SJ, Lowenstein DH, Skarnes WC, Chedotal A, Tessier-Lavigne M (2000) Neuropilin-2 regulates the development of selective cranial and sensory nerves and hippocampal mossy fiber projections. Neuron 25:43–56.

Chen XJ, Kovacevic N, Lobaugh NJ, Sled JG, Henkelman RM, Henderson JT (2006) Neuroanatomical differences between mouse strains as shown by high-resolution 3D MRI. Neuroimage 29:99–105.

Chen ZY, Sun C, Reuhl K, Bergemann A, Henkemeyer M, Zhou R (2004) Abnormal hippocampal axon bundling in EphB receptor mutant mice. J Neurol Sci 24:2366–2374.

Cowan CA, Henkemeyer M (2002) Ephrins in reverse, park and drive. Trends Cell Biol 12:339–346.

Cowan CA, Yokoyama N, Bianchi LM, Henkemeyer M, Fritzsch B (2000) EphB2 guides axons at the midline and is necessary for normal vestibular function. Neuron 26:417–430.

Cowan CA, Yokoyama N, Saxena A, Chumley MJ, Silvany RE, Baker LA, Srivastava D, Henkemeyer M (2004) Ephrin-B2 reverse signaling is required for axon pathfinding and cardiac valve formation but not early vascular development. Dev Biol 271:263–271.

Cunningham MG, McKay RD (1993) A hypothermic miniaturized stereotaxic instrument for surgery in newborn rats. J Neurosci Methods 47:105–114.

Davy A, Robbins SM (2000) Ephrin-A5 modulates cell adhesion and morphology in an integrin-dependent manner. EMBO J 19:5396–5405.

Davy A, Soriano P (2005) Ephrin signaling in vivo: look both ways. Dev Dyn 232:1–10.

Davy A, Soriano P (2007) Ephrin-B2 forward signaling regulates somite patterning and neural crest cell development. Dev Biol 304:182–193.

Day B, To C, Himanen JP, Smith FM, Nikolov DB, Boyd AW, Lackmann M (2005) Three distinct molecular surfaces in ephrin-A5 are essential for a functional interaction with EphA3. J Biol Chem 280:26526–26532.

Dickson BJ, Gilestro GF (2006) Regulation of commissural axon pathfinding by slit and its Robo receptors. Annu Rev Cell Dev Biol 22:651–675.

Dodd J, Jessell TM (1988) Axon guidance and the patterning of neuronal projections in vertebrates. Science 242:692–699.

Dottori M, Hartley L, Galea M, Paxinos G, Polizzotto M, Kilpatrick T, Bartlett PF, Murphy M, Kontgen F, Boyd AW (1998) EphA4 (Sek1) receptor tyrosine kinase is required for the development of the corticospinal tract. Proc Natl Acad Sci U S A 95:13248–13253.

Dufour A, Seibt J, Passante L, Depaepe V, Ciossek T, Frisen J, Kullander K, Flanagan JG, Polleux F, Vanderhaeghen P (2003) Area specificity and topography of thalamocortical projections are controlled by ephrin/Eph genes. Neuron 39:453–465.

Elowe S, Holland SJ, Kulkarni S, Pawson T (2001) Downregulation of the Ras-mitogen-activated protein kinase pathway by the EphB2 receptor tyrosine kinase is required for ephrin-induced neurite retraction. Mol Cell Biol 21:7429–7441.

Falk J, Bechara A, Fiore R, Nawabi H, Zhou H, Hoyo-Becerra C, Bozon M, Rougon G, Grumet M, Puschel AW, Sanes JR, Castellani V (2005) Dual functional activity of semaphorin 3B is required for positioning the anterior commissure. Neuron 48:63–75.

Franklin K, Paxinos G (1997) The mouse brain in stereotaxic coordinates. Academic Press.

Frisen J, Yates PA, McLaughlin T, Friedman GC, O'Leary DD, Barbacid M (1998) Ephrin-A5 (AL-1/RAGS) is essential for proper retinal axon guidance and topographic mapping in the mammalian visual system. Neuron 20:235–243.

Gale NW, Baluk P, Pan L, Kwan M, Holash J, DeChiara TM, McDonald DM, Yancopoulos GD (2001) Ephrin-B2 selectively marks arterial vessels and neovascularization sites in the adult, with expression in both endothelial and smooth-muscle cells. Dev Biol 230:151–160.

Gale NW, Holland SJ, Valenzuela DM, Flenniken A, Pan L, Ryan TE, Henkemeyer M, Strebhardt K, Hirai H, Wilkinson DG, Pawson T, Davis S, Yancopoulos GD (1996) Eph receptors and ligands comprise two major specificity subclasses and are reciprocally compartmentalized during embryogenesis. Neuron 17:9–19.

Gao PP, Sun CH, Zhou XF, DiCicco-Bloom E, Zhou R (2000) Ephrins stimulate or inhibit neurite outgrowth and survival as a function of neuronal cell type. J Neurosci Res 60:427–436.

Giger RJ, Cloutier JF, Sahay A, Prinjha RK, Levengood DV, Moore SE, Pickering S, Simmons D, Rastan S, Walsh FS, Kolodkin AL, Ginty DD, Geppert M (2000) Neuropilin-2 is required in vivo for selective axon guidance responses to secreted semaphorins. Neuron 25:29–41.

Greferath U, Canty AJ, Messenger J, Murphy M (2002) Developmental expression of EphA4-tyrosine kinase receptor in the mouse brain and spinal cord. Gene Expr Patterns 2:267–274.

Guilfoyle DN, Dyakin VV, O'Shea J, Pell GS, Helpern JA (2003) Quantitative measurements of proton spin-lattice (T1) and spin-spin (T2) relaxation times in the mouse brain at 7.0 T. Magn Reson Med 49:576–580.

Henkemeyer M, Orioli D, Henderson JT, Saxton TM, Roder J, Pawson T, Klein R (1996) Nuk controls pathfinding of commissural axons in the mammalian central nervous system. Cell 86:35–46.

Himanen JP, Chumley MJ, Lackmann M, Li C, Barton WA, Jeffrey PD, Vearing C, Geleick D, Feldheim DA, Boyd AW, Henkemeyer M, Nikolov DB (2004) Repelling class discrimination: ephrin-A5 binds to and activates EphB2 receptor signaling. Nat Neurosci 7:501–509.

Hindges R, McLaughlin T, Genoud N, Henkemeyer M, O'Leary DD (2002) EphB forward signaling controls directional branch extension and arborization required for dorsal-ventral retinotopic mapping. Neuron 35:475–487.

Iwasato T, Katoh H, Nishimaru H, Ishikawa Y, Inoue H, Saito YM, Ando R, Iwama M, Takahashi R, Negishi M, Itohara S (2007) Rac-GAP alpha-chimerin regulates motor-circuit formation as a key mediator of EphrinB3/EphA4 forward signaling. Cell 130:742–753.

Knoll B, Zarbalis K, Wurst W, Drescher U (2001) A role for the EphA family in the topographic targeting of vomeronasal axons. Development 128:895–906.

Kovacevic N, Henderson JT, Chan E, Lifshitz N, Bishop J, Evans AC, Henkelman RM, Chen XJ (2005) A three-dimensional MRI atlas of

the mouse brain with estimates of the average and variability. Cereb Cortex 15:639–645.
Kudo C, Ajioka I, Hirata Y, Nakajima K (2005) Expression profiles of EphA3 at both the RNA and protein level in the developing mammalian forebrain. J Comp Neurol 487:255–269.
Kullander K, Mather NK, Diella F, Dottori M, Boyd AW, Klein R (2001) Kinase-dependent and kinase-independent functions of EphA4 receptors in major axon tract formation in vivo. Neuron 29:73–84.
Mann F, Peuckert C, Dehner F, Zhou R, Bolz J (2002) Ephrins regulate the formation of terminal axonal arbors during the development of thalamocortical projections. Development 129:3945–3955.
Marquardt T, Shirasaki R, Ghosh S, Andrews SE, Carter N, Hunter T, Pfaff SL (2005) Coexpressed EphA receptors and ephrin-A ligands mediate opposing actions on growth cone navigation from distinct membrane domains. Cell 121:127–139.
Miao J, Vitek MP, Xu F, Previti ML, Davis J, Van Nostrand WE (2005) Reducing cerebral microvascular amyloid-beta protein deposition diminishes regional neuroinflammation in vasculotropic mutant amyloid precursor protein transgenic mice. J Neurol Sci 25:6271–6277.
Mori S, Zhang J (2006) Principles of diffusion tensor imaging and its applications to basic neuroscience research. Neuron 51:527–539.
Neema M, Stankiewicz J, Arora A, Dandamudi VS, Batt CE, Guss ZD, Al-Sabbagh A, Bakshi R (2007) T1- and T2-based MRI measures of diffuse gray matter and white matter damage in patients with multiple sclerosis. J Neuroimaging 17 (Suppl 1):16S–21S.
Negishi M, Oinuma I, Katoh H (2005) Plexins: axon guidance and signal transduction. Cell Mol Life Sci 62:1363–1371.
Nessler S, Boretius S, Stadelmann C, Bittner A, Merkler D, Hartung HP, Michaelis T, Bruck W, Frahm J, Sommer N, Hemmer B (2007) Early MRI changes in a mouse model of multiple sclerosis are predictive of severe inflammatory tissue damage. Brain 130:2186–2198.
O'Leary DD, Wilkinson DG (1999) Eph receptors and ephrins in neural development. Curr Opin Neurobiol 9:65–73.
Otal R, Burgaya F, Frisen J, Soriano E, Martinez A (2006) Ephrin-A5 modulates the topographic mapping and connectivity of commissural axons in murine hippocampus. Neuroscience 141:109–121.
Pabbisetty KB, Yue X, Li C, Himanen JP, Zhou R, Nikolov DB, Hu L (2007) Kinetic analysis of the binding of monomeric and dimeric ephrins to Eph receptors: correlation to function in a growth cone collapse assay. Protein Sci 16:355–361.
Palmer A, Klein R (2003) Multiple roles of ephrins in morphogenesis, neuronal networking, and brain function. Genes Dev 17:1429–1450.
Palmer A, Zimmer M, Erdmann KS, Eulenburg V, Porthin A, Heumann R, Deutsch U, Klein R (2002) EphrinB phosphorylation and reverse signaling: regulation by Src kinases and PTP-BL phosphatase. Mol Cell 9:725–737.
Park TS, Lee SY (2007) Effects of neuronal magnetic fields on MRI: numerical analysis with axon and dendrite models. Neuroimage 35:531–538.
Pasquale EB (2004) Eph-ephrin promiscuity is now crystal clear. Nat Neurosci 7:417–418.
Sahay A, Molliver ME, Ginty DD, Kolodkin AL (2003) Semaphorin 3F is critical for development of limbic system circuitry and is required in neurons for selective CNS axon guidance events. J Neurol Sci 23:6671–6680.
Serafini T, Colamarino SA, Leonardo ED, Wang H, Beddington R, Skarnes WC, Tessier-Lavigne M (1996) Netrin-1 is required for commissural axon guidance in the developing vertebrate nervous system. Cell 87:1001–1014.
Stein E, Savaskan NE, Ninnemann O, Nitsch R, Zhou R, Skutella T (1999) A role for the Eph ligand ephrin-A3 in entorhino-hippocampal axon targeting. J Neurol Sci 19:8885–8893.
Wang HU, Anderson DJ (1997) Eph family transmembrane ligands can mediate repulsive guidance of trunk neural crest migration and motor axon outgrowth. Neuron 18:383–396.
Wegmeyer H, Egea J, Rabe N, Gezelius H, Filosa A, Enjin A, Varoqueaux F, Deininger K, Schnutgen F, Brose N, Klein R, Kullander K, Betz A (2007) EphA4-dependent axon guidance is mediated by the RacGAP alpha2-chimaerin. Neuron 55:756–767.
Wilkinson DG (2000) Eph receptors and ephrins: regulators of guidance and assembly. Int Rev Cytol 196:177–244.
Wilkinson DG (2001) Multiple roles of EPH receptors and ephrins in neural development. Nat Rev Neurosci 2:155–164.
Woods RP, Grafton ST, Holmes CJ, Cherry SR, Mazziotta JC (1998) Automated image registration. I. General methods and intrasubject, intramodality validation. J Comput Assist Tomogr 22:139–152.
Wybenga-Groot LE, Baskin B, Ong SH, Tong J, Pawson T, Sicheri F (2001) Structural basis for autoinhibition of the Ephb2 receptor tyrosine kinase by the unphosphorylated juxtamembrane region. Cell 106:745–757.
Yue Y, Chen ZY, Gale NW, Blair-Flynn J, Hu TJ, Yue X, Cooper M, Crockett DP, Yancopoulos GD, Tessarollo L, Zhou R (2002) Mistargeting hippocampal axons by expression of a truncated Eph receptor. Proc Natl Acad Sci U S A 99:10777–10782.
Zhou X, Suh J, Cerretti DP, Zhou R, DiCicco-Bloom E (2001) Ephrins stimulate neurite outgrowth during early cortical neurogenesis. J Neurosci Res 66:1054–1063.

(Accepted 5 March 2009)
(Available online 13 March 2009)